Journal of Thermal Analysis and Calorimetry (2022) 147:11313–11330
https://doi.org/10.1007/s10973-022-11295-7

Numerical investigation on the performance of the double tube heat exchangers with different tube geometries and Turbulators

Mohammad Ravanbakhsh[1] · Mahdi Deymi-Dashtebayaz[1] · Mojtaba Rezapour[1]

Received: 9 December 2021 / Accepted: 24 February 2022 / Published online: 10 April 2022

Abstract

In the present work, heat transfer and fluid flow in simple tube geometry, star-shaped tube geometry, and turbulator inserted geometry have been investigated and compared. Also, it is located in a double tube heat exchanger to use in a residential gas fire water heater. The most critical parameters are considered including temperature distribution, Nusselt number, convective heat transfer coefficient, coefficient of friction, and pressure drop. The simulation is 3D, and the SIMPLE algorithm is used for numerical solution based on the finite volume method. Then, by considering two methods of changing the geometry of the tube and using a turbulator in the flow path to increase the efficiency of a double tube heat exchanger and comparing them with each other, the most optimal case is presented. The validation is shown acceptable agreement by the absolute average deviation (AAD) error of 7.13% compared to the experimental data and numerical results. In the $200 \leq \mathrm{Re} \leq 1800$ for cold flow and the constant Reynolds number equal to 1800 for hot flow, the results show that when using heat exchanger geometries with turbulator and star-shaped tube instead of the simple heat exchanger geometry, the Nusselt number on either the hot or cold side of the heat exchanger has improved up to 146% and 50%, respectively. For cold flow in turbulator inserted geometry, in the best result, the Nusselt number increased 2.4 times to 6.107, and for star-shaped tube geometry up 1.5 times to 3.939. For hot flow in turbulator inserted geometry, the Nusselt number has increased up to 48.05, and for star-shaped, tube geometry decreased to 16.3 in comparison to simple geometry. In addition, the pressure drop for the cold side of the flow in the mode of the simple double tube and the coiled wire double tube is approximately identical (maximum 1818.06 for $\mathrm{Re} = 1800$), while the pressure drop in the double star-shaped tubes is reduced by up to 50% compared to the other two modes and its best value at $\mathrm{Re} = 1800$ is 1419.94pa. Finally, by using the Topsis method, as a multi-objective optimization technique, and according to the two criteria with different mass, including pressure drop, as an undesirable criterion, and Nusselt number, as a desirable criterion, the optimal Reynolds number for cold flow was determined.

Keywords Double tube heat exchanger, Computational fluid dynamics (CFD) · Coiled wire insert · Friction factor · Geometry · Multi-objective optimization

List of symbols

A	Area (m^2)
A_{hf}	Heat transfer surface area (m^2)
c_p	Heat capacity (kJ $kg^{-1}K^{-1}$)
d_c	Diameter of outside tube (Cold flow) (*mm*)
d_h	Diameter of inside tube (Hot flow) (*mm*)
d_i	Diameter of coil wire (*mm*)
d_m	Small diameter of Ellipsoid (*mm*)
D_H	Hydraulic diameter (*mm*)
D_L	Large diameter of Ellipsoid (*mm*)
e	Internal energy (*J*)
f	Friction coefficient
h	Heat transfer coefficient (W $m^{-2}K^{-1}$)
H	Enthalpy (*J*)
$\mathbf{J}$	Diffusion flux (kg $m^{-2}s^{-1}$)
k	Thermal conductivity (W $m^{-1}K^{-1}$)
K	Turbulent kinetic energy (*J*)
L	Tube length (*mm*)
$\dot{m}$	Mass flow rate (kg s^{-1})
Nu	Nusselt number
p	Pressure (*Pa*)
P	Pitch length of coil wire (*mm*)
Re	Reynolds number
S	Perimeter (*m*)
t	Tube thickness (*mm*)
T	Temperature (*K*)

✉ Mahdi Deymi-Dashtebayaz
m.deimi@hsu.ac.ir; meh_deimi@yahoo.com

[1] Center of Computational Energy, Department of Mechanical Engineering, Hakim Sabzevari University, Sabzevar, Iran

T_∞ Reference temperature (K)
T_s Calculated temperature (K)
$\mathbf{v}$ Flow Velocity (m s^{-1})

Greek symbols

μ Dynamic viscosity (kg $m^{-1}s^{-1}$)
μ_t Turbulent dynamic viscosity (kg $m^{-1}s^{-1}$)
υ Kinematic viscosity (m^2s^{-1})
ρ Mass density (kg m^{-3})
τ Deviatoric stress tensor (N mm^{-2})
ε Turbulent kinetic energy dissipation rate (m^2s^{-3})
θ^* Dimensionless temperature

Subscripts

$A.A$ Area average
C, c Cold flow
H, h Hot flow
$r-c$ Cold flow ratio
$r-h$ Hot flow ratio
lm Logarithmic mean
i Inlet
o Outlet

Introduction

Today, with the extension of petroleum derivative utilization and the subsequent issues, including a worldwide temperature alteration and air contamination, it is important to concentrate on techniques to lessen the utilization of these energy sources generally. In Iran, ambient heating and consumption of domestic hot water devices account for 70.53% and 24.21% of the total residential consumption of natural gas, respectively [1]. Under these conditions, the utilization of private gas fire water radiators has filled fundamentally as of late, and private houses are all the while liable for encompassing warming and homegrown boiling water, something that accounts for a large portion of domestic natural gas consumption. The residential gas fire water heater uses natural gas to provide the necessary heat for ambient heating and hot water for sanitary purposes. The heat exchange is the main component of combustion products to the water. Double tube heat exchangers are one of the most common heat the residential gas fire water heater, which is responsible for transferring heat from the combustion of gas from air and combustion products to water. Double tube heat exchangers are one of the most common heat exchangers used in a residential gas fire water heater, which are widely used in small industries due to their low cost of design, maintenance. Also, due to the low efficiency of this type of heat exchanger, it is important to provide methods to improve heat transfer. Investigating and optimizing this important matter can increase the thermal efficiency of residential gas fire water heaters and various industries. In addition, it considerably reduces fuel consumption and greenhouse gas emissions. At present, two-third share of carbon dioxide production has been consumed based on the COP21 goal, and the remaining amount will be exhausted by 2050 [2]. Various methods have been studied to increase the efficiency of this type of heat exchanger. One of these methods is turbulent the thermal boundary layer by using a turbulator in the fluid flow. Turbulators can be used in the form of simple longitudinal strips [3], twisted tapes [4–6], coil wire [7] or any other creative geometry [8]. Other methods that can be mentioned are increasing the heat transfer area by using baffles [9], changing the geometry of heat exchangers [10] and the use of nanofluids as operating fluid [11].

A wide range of nanofluids is used for this purpose. In some of studies, water is used as a base fluid, and metals such as AL_2O_3 [12–14] and carbon [15] are used as nanoparticles but in other studies, other fluids such as hybrid fluids [16], graphene [17–19] and gallium [20] are used as a base fluid. For example, Li et al. [21] experimentally investigated the effect of using carbon-acetone nanofluid on the performance of heat exchangers, and the result showed 73% improvement in hydraulic and thermal performance. Alazwari and Safaei [22] numerically showed the use of nanofluids and changing the angle of the baffles in a shell and tube heat exchanger will improve heat transfer.

Mainly star-shaped tubes have been used to increase efficiency in double tube heat exchangers used in residential gas-fire water heater [23]. In the current article, this design has been studied as one of the geometries problems. In the following part, we will review the articles that have been done to improve the efficiency of this category of heat exchangers.

Numerical studies

In recent decades, numerical simulation and modeling of heat exchangers from the perspective of heat transfer and fluid flow has received special attention. In this regard, Abu-Hamed et al. [24] numerically studied the heat transfer and flow parameters in a double tube micro-heat exchanger with smooth and helix paths and different pitch and turn rotations. By increasing the Reynolds number of heat transfers, the heat transfer is improved in the helix path and at any angle, and pressure drop and pump operation are increased. The highest overall coefficient of heat transfer and effectiveness in Reynolds number 200 and pitch 2 are 45% and 11.5%, respectively. In the same conditions, the pressure drop, pump operation and coefficient of friction 42% are increased. Monfared et al. [25] has numerically investigated the effect of helical ribs as turbulators and different nanofluid concentrations on heat transfer in a tube. The use of turbulator compared to the simple state at Re = 250, the Nusselt number and the coefficient of friction showed up to 40%

and 80% increase in flow, respectively. Deymi-Dashtebayaz et al. [26] analytically investigated and optimized the new heat exchangers that were drilled on it. Comprehensive sensitivity analysis of thermo-hydraulic parameters and optimization of Cuo/water nanofluid flow flowing inside the heat exchanger was performed. The results showed that the average flow temperature and the pitch ratio of the cavities had the least and the greatest effect on the reduction in production entropy, respectively. Yang et al. [27] used a mathematical model to simulate several models of heat transfer improvers and then optimized the size of the tube and shell and tube heat exchanger. The results show that by increasing the heat transfer rate, the final cost of the heat exchanger is reduced by up to 20.4% when using a coiled wire turbulator.

Nakhchi and Esfahani [28] the effect of double V - cut twisted tapes as a turbulator was investigated and CuO-water nanofluid was used as the operating fluid. Heat transfer improved up to 14.5% for 1.5% nanofluid concentration. Cutting in turbulator improved Nusselt number by 138% compared to simple turbulator. Shahsavar Goldanlou et al. [29] the effect of blade-shape turbulator on forced convection heat transfer in shell and tube heat exchanger has investigated. The results showed that by increasing blade-rod diameter, the performance evaluation criterion first increases and then decreases. Most PEC occurred at Re = 9000 and blade-rod diameter of 15 mm.

Sharifi et al. [30] have numerically investigated the use of coiled wire in the double tube heat exchanger, its effect on Nusselt number, coefficient of friction, and final efficiency of this type of heat exchangers. The results show that the Nusselt number improves up to 1.77 times, and the coefficient of friction increases. The best efficiency is obtained when a balance is established between the Nusselt number and the coefficient of friction. Paneliya et al. [31] have numerically studied the temperature parameters in a double tube heat exchanger in which two different types of turbulators, including twist metal tape and X-tape, have been used. The X-tape shows a better thermal performance than the twist-tape and increases the heat transfer rate by 1.27 times compared to the twist-tape. Nakhchi and Esfahani [32] have numerically studied the flow of copper and water nanofluids and the heat transfer of these nanofluids in a heat exchanger. Inside the heat exchanger, a special geometry of the twist-tape is used as a turbulator. The effect of the geometric parameters of this turbulator was also investigated, which showed that the heat transfer coefficient increased to 23.20% and is directly related to the volumetric quality of nanoparticles. Rashidi et al. [33] numerically, have studied the effect of the turbulent model of the twist-tape model and its deviation from the center of the tube, inflow, heat, and production entropy. During the highest heat transfer, the entropy of heat production and friction increased to 237% and 42%, respectively.

Experimental studies

Due to the widespread use of heat exchangers and the importance of improving their efficiency in industry, many studies and experiments have been performed experimentally in this field. In this regard, Emani et al. [34] used various geometries and techniques experimentally to reduce the size of the heat exchanger and increase the heat transfer rate. The results showed that the changes in coefficient of friction and Nusselt number are directly related to Reynolds number changes and are affected by channel shape, helix angle, and wire diameter. Yu et al. [35] have numerically studied the kinematic heat transfer heat in a tube, which in addition to rotating clockwise and counterclockwise, in their design, coiled wires with different geometric sections have been used. The results show that the simultaneous use of both techniques improves heat transfer rate and pump consumption. Sinaga et al.[36] experimentally investigated the injection of air into the inner tube flow of a double tube heat exchanger. Energy and exergy parameters were studied and the heat transfer coefficient was increased up to 33% and the number of heat transfer units up to 38%. Panahi and Zamzamian [37] experimentally investigated the effect of a turbulator on a twisted shell and tube heat exchanger. The use of a turbulator improved heat transfer and increased pressure drop.

Moghaddam et al. [38, 39] experimentally investigated the heat transfer characteristics, flow pattern and pressure drop during condensation r600a in the tube with a coiled wire turbulator. At best, they were able to increase the heat transfer coefficient by up to 107%, and lower steam quality was observed than normal. The pressure drop is increased up to 11.97 times compared to the normal case, and by decreasing the wire diameter and increasing the pitch of coiled wire, the pressure drop decreases, which has improved the system performance at high mass flow rates. Raei et al. [40] used the design of a new method to calculate the transfer coefficient of heat transfer in the double tube heat exchanger and experimentally tested its accuracy. This study showed that there is a significant difference between the results of these methods and indicates the dependence of the Nusselt number on Reynolds number. Gonzalez et al. [41] experimentally investigated the effect of using a coiled wire turbulator on the external layer of the inner tube on the double tube heat exchanger and pressure reduction in double tube heat exchangers. According to the obtained results, the use of turbulator improves heat transfer and at the same time increases the pressure drop compared to the simplified state, but with increasing Reynolds number (more than 5500) the effect of coiled wire in increasing heat transfer decreases. He et al. [42] have experimentally investigated the effect of using a particular type of turbulator on heat transfer and coefficient of friction. The results showed that the Nusselt number and

the coefficient of friction first decrease and then increase. This method increases the Nusselt number up to 120% and the coefficient of friction up to 10 times and increases the overall performance of the system from 0.87 to 0.98 times. Kumar et al. [43] have experimentally investigated a type of energy storage device that by placing coiled wires in the path of hot air flow, they were able to increase the efficiency of the source from 76.9% in the simple case to 85.9% when using the coiled wire. Singh and Sarkar [44] have experimentally investigated the use of retractable and opening coiled wire in a double tube heat exchanger used for hybrid nanofluid cooling. According to the results, the opening geometry has better thermal performance than other geometries and the pressure drop has improved when using any of the geometries used in this research. Keklikcioglu and Ozceyhan [45] experimentally investigated the hydrothermal performance of using a coiled wire turbulator with a square cross section in a tube so that the coiled wire was 1 mm away from the inner wall of the tube along the entire flow path. The results showed that in the best conditions, compared to the simple state without a turbulator, the thermal efficiency increased up to 1.67 times. Moya-Rico et al. [46] experimentally investigated the effect of using a short-length twist-tape turbulator and applying a number of them with different arrangements for different Reynolds numbers in the flow path of a double tube heat exchanger that increased heat transfer. The result was that if the distance between the turbulators increases, the Nusselt number decreases, but the pitch of a turbulator has less effect on the thermal efficiency compared to the operating conditions of the exchanger. Keklikcioglu and Ozceyhan [47] experimentally investigated the entropy generated and the heat transfer in a tube containing a coiled wire and identical triangle geometries that were responsible for creating a distance between the tube and the coiled wire during different Reynolds number flows. As Reynolds number increases, the production entropy increases, and as the diameter of the coiled wire decreases, the production entropy decreases. Li et al. [48] have experimentally investigated the flow of water and gas fluid into a horizontal tube and the use of a coiled wire turbulator inside it. When using a turbulator, the efficiency of the heat exchanger is increased, but compared to the simple state without a coiled wire, the temperature changes are more uniform. In this case, increasing the mass flow rate increases the thermal efficiency, and the heat transfer coefficient increases by 2.5 to 3.5 times on average. Vaisi et al. [49] experimentally investigated heat transfer and pressure drop in the double tube heat exchanger in which a twist-tape was used inside the inner tube. In this experiment, different types of turbulator geometry with simple separators and separators with holes with different geometries were examined for different Reynolds numbers. In the case of using a twist-tape with a separator, compared to the simple case, the heat transfer improved and the pressure drop decreased, and when using a twist-tape with a separator on which holes were made. In particular, in a circular geometry, more heat transfer and less pressure drop were shown. Ribeiro et al. [50] experimentally investigated the effect of a turbulator on the hot part of a radiator and found that the use of a turbulator significantly improved system performance. Goh et al. [51] experimentally investigated the exposure of a particular type of turbulator and the effect of its rotation on the improvement of heat transfer and the generated entropy of forced heat transfer. The Nusselt number improved for both modes, but showed better performance for the rotating mode, and by observing lower entropy production in the rotating mode, this method performed better overall from the two perspectives of improving heat transfer and the second law of thermodynamics.

Novelty and motivation

According to studies, although research to improve heat transfer in a double tube heat exchanger by changing the geometry of the tube or using a turbulator in the flow path has been done numerically and experimentally. However, the effects of these two methods on the different parameters of flow and heat transfer, are not properly compared. The widespread use of these two methods in heat exchangers of gas-fire water heater, increases the importance of investigating heat transfer between cold fluid (or heating system flow) and hot fluid (or sanitary water flow). In addition, according to the circulation of the fluid by using the pump in the path of the heating system, the optimal velocity of the fluid is just as important as heat transfer. Therefore, the parametric study from a thermal and fluid point of view is very important in this field. In this work, to increase the efficiency of double tube heat exchanger used in the residential gas fire water heater, a comprehensive parametric comparison of heat transfer and fluid flow between three different models of double tube heat exchanger has been done, and finally, the most optimal model has been introduced. The independence of the network is examined after validation of the results obtained from numerical simulation. Then the fluid flow and heat transfer characteristics including pressure drop, friction coefficient, temperature changes, and Nusselt number in each geometry are presented and examined and compared with each other. The effect of each geometry on pressure drop, temperature changes, and thermal performance in different Reynolds numbers is investigated and the optimal method is introduced by setting the parameters of heat transfer and pressure drop. Then, by using the Topsis method, and considering various masses for the two criteria of pressure drop and Nusselt number, the optimal Reynolds number for the proper operation of the heat exchanger has been calculated.

Problem description

In this research, the fluidity and heat of double tube heat exchangers with different geometries along with turbulators have been investigated. The parameters of pressure drop and velocity distribution as flow parameters and Convection Heat Transfer Coefficient with Nusselt number as the most important parameters on the different geometry of double tube heat exchangers have been studied. Figure 1 shows the illustrations of the geometry of a double tube heat exchanger with three different geometries. These geometries include, respectively, a. double tube heat exchanger with simple tube geometry, b. double tube heat exchanger with turbulator, and c. star-shaped double tube heat exchanger. For all specified geometries, the length of the heat exchanger is equal to L and has the same cross-sectional area for the cold side with A_C and the hot side with A_H. Also, this study aims to use modeled heat exchangers in the residential gas fire water heater. As shown in Figure 2, the dimensions considered in this regard have been selected.

In this modeling, the flow is considered as counter flow. The hydraulic diameter is equal to d_h for internal flow and d_c for external flow. In the internal flow path of geometry B, a coiled wire with a coiled pitch P and a cross-sectional area of diameter d_i has been used as a turbulator to disturb the flow and improve heat transfer. Geometry C has an elliptical cross section with a large diameter d_L and a small diameter d_m. It is worth noting that to compare in the same and boundary conditions, the cross-sectional area of all three geometries is equal for internal and external flow. The thickness of the tube is considered t equally in all geometries.

According to Fig. 3 in geometry A, the cold fluid flow enters the outer tube, and hot fluid enters the inner tube. The inlet temperatures of hot and cold fluids are equal to $T_{C,i}$ and $T_{H,i}$, and their outlet temperatures are equal to $T_{C,o}$ and $T_{H,o}$. The Cold and hot fluid temperatures are T_C and T_H, respectively. Therefore, the computational range is considered to investigate heat transfer only from hot to the cold fluid. Conductive heat transfer in the inner tube wall is also effective. The temperature of the tube wall is T_W. A_H, and A_C are the cross section of hot and cold flow, respectively.

D_H is the hydraulic diameter of the channel through which water flows. It is defined by $D_{H,c}$ and $D_{H,h}$ for cold and hot flow, respectively.

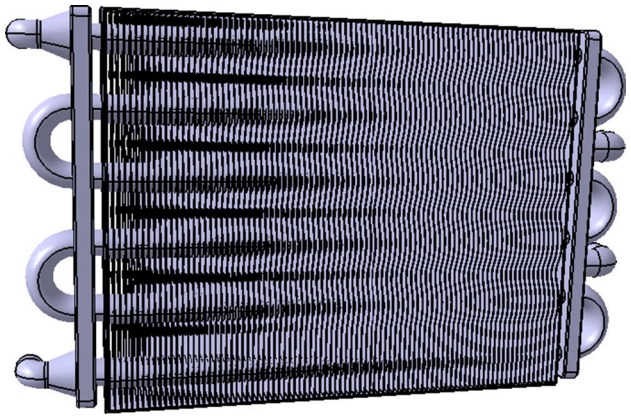

Fig. 2 Example of a heat exchanger used in a residential gas-fired water heater

The governing equations

In this section, the equations and boundary conditions that govern numerical solution and optimization equations based on the TOPSIS method are introduced**.**

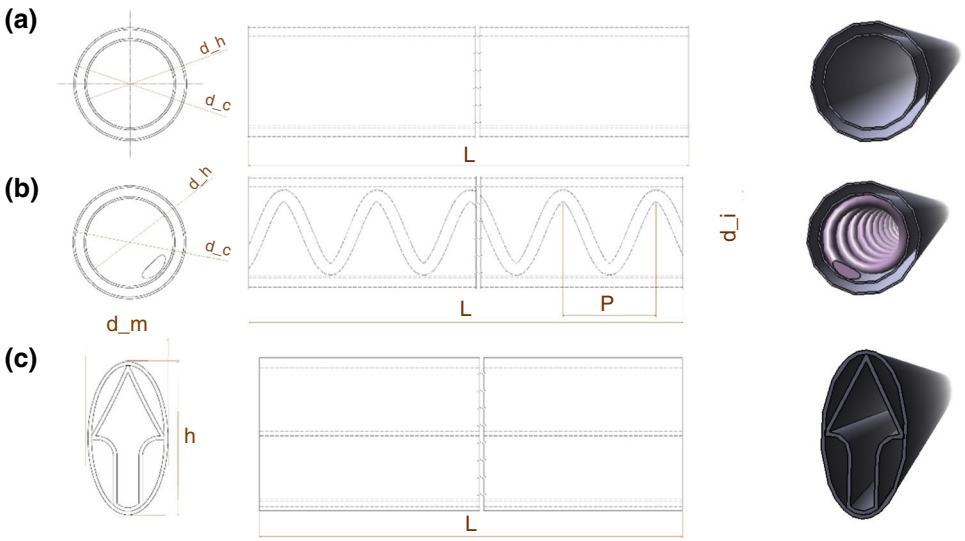

Fig. 1 The geometries reviewed in the present study include **a** simple tube geometry, **b** turbulator inserted geometry, and **c** star-shaped tube geometry

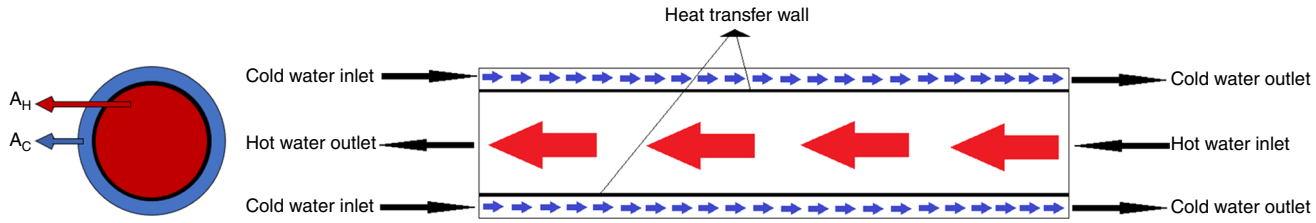

Fig. 3 The path and cross section of the hot and cold flow inside the double tube heat exchanger

Equations of numerical solution

The governing equations in the numerical solution include the equation of Navier–Stokes for fluid flow and the equation of energy for investigating heat transfer. This simulation is performed in 3-D, steady-state, and incompressible flow conditions. The fluid is also incompressible, and volumetric forces are ignored. The equation of continuity and momentum is given by Eq. (1) and (2), respectively.

$$\nabla \cdot \left(\rho \vec{v}\right) = 0 \tag{1}$$

$$\nabla \cdot \left(\rho \vec{v}\vec{v}\right) = -\nabla p + \tau \tag{2}$$

$$\tau = \mu\left(\nabla \vec{v} + \left(\nabla \vec{v}\right)^{\mathrm{T}}\right) \tag{3}$$

Therefore, ρ, $\vec{v}$, p, and τ are density, flow velocity, fluid pressure, and shear stress tensor, respectively.

To model, the flow regime and thermal boundary layer in geometry B and the turbulence flow are created by the turbulator, the standard k-ε turbulence model with 5% turbulence intensity is used [52]. The governing equations of this type of flow are expressed as follows:

$$\nabla \cdot (\rho \vec{v} K) = \nabla \cdot \left(\left(\mu + \frac{\mu_{\mathrm{t}}}{\sigma_{\mathrm{K}}}\right)\nabla K\right) + G_{\mathrm{K}} - \rho\varepsilon \tag{4}$$

$$\nabla \cdot (\rho \vec{v} \varepsilon) = \nabla \cdot \left(\left(\mu + \frac{\mu_{\mathrm{t}}}{\sigma_{\varepsilon}}\right)\nabla \varepsilon\right) + C_{\varepsilon 1}\frac{\varepsilon}{K}G_{\mathrm{k}} - \rho C_{\varepsilon 2}\frac{\varepsilon^2}{K} \tag{5}$$

$$\mu_{\mathrm{t}} = \rho C_{\mu}\frac{K^2}{\varepsilon} \tag{6}$$

$$G_{\mathrm{k}} = \mu_{\mathrm{t}}\left[\nabla \vec{v} : \left(\nabla \vec{v} + \left(\nabla \vec{v}\right)^{t}.\frac{2}{3}\rho K \nabla \cdot \vec{v}\right)\right] - \frac{2}{3}\rho K \nabla \cdot \vec{v} \tag{7}$$

K is the term of turbulent kinetic energy, μ_{t} is the dynamic viscosity coefficient of turbulence, ε is the rate of dissipation, G_{K} is the kinetic energies produced by turbulent flows are moderate and $C_{\varepsilon 1}, C_{\varepsilon 2}, C_{\mu}$ is constant due to changes in velocity. σ_{K} and σ_{ε} are the values of the turbulent flow Prandtl number for K and ε. υ is the kinematic viscosity of the fluid. The energy equation is as follows:

$$\rho C_{\mathrm{P}} \vec{v} \cdot \nabla T = \nabla \cdot (k \nabla T) \tag{8}$$

Therefore, T is temperature, k is thermal conductivity, and C_{p} represents heat capacity. For geometry A in low Reynolds numbers ($200 \leq \mathrm{Re} \leq 1800$), the turbulence term is omitted because of the flow is considered smooth. In Eq. (9), the coefficient of friction is obtained from the pressure difference between the inlet and outlet sides of the flow in hot and cold flow. ΔP indicates the pressure difference between the input and output currents on each of the currents. L is indicated by the length of the heat exchanger.

$$f = \frac{\Delta P}{\left(\frac{L}{D_{\mathrm{H}}}\right)\left(\frac{\rho V^2}{2}\right)} \tag{9}$$

D_{H} indicates the hydraulic diameter, which is also used to calculate the Reynolds number. The hydraulic diameter calculation equation and other additional equations are described in Appendix A.

According to Eq. (10), ΔT_{lm} shows the logarithmic mean of the temperature difference between the double tube heat exchangers. $T_{\mathrm{h,i}}$ is the inlet temperature of the hot stream, $T_{\mathrm{C,i}}$ is the inlet temperature of the cold stream, $T_{\mathrm{h,o}}$ is the outlet temperature of the hot stream, and $T_{\mathrm{C,o}}$ is the outlet temperature of the cold stream.

$$\Delta T_{\mathrm{lm}} = \frac{\left(T_{\mathrm{H,i}} - T_{\mathrm{C,o}}\right) - \left(T_{\mathrm{H,o}} - T_{\mathrm{C,i}}\right)}{Ln\left(\frac{T_{\mathrm{H,i}} - T_{\mathrm{C,o}}}{T_{\mathrm{H,o}} - T_{\mathrm{C,i}}}\right)} \tag{10}$$

h is the heat transfer coefficient at which $\dot{m}$ is the rate of flow, c_{p} is Special heat, $\mathrm{A_{hf}}$ is the surface area through which heat is transferred. The heat transfer coefficient is defined for cold flow with $\mathrm{h_c}$ and hot flow with $\mathrm{h_h}$.

$$h = \frac{\dot{m} c_{\mathrm{p}}\left(T_{\mathrm{in}} - T_{\mathrm{out}}\right)}{A_{\mathrm{hf}}\Delta T_{\mathrm{lm}}} \tag{11}$$

The Nusselt number is also shown for cold flow with $\mathrm{Nu_c}$ and hot flow with $\mathrm{Nu_h}$.

$$Nu = \frac{hD_{\mathrm{H}}}{k} \tag{12}$$

The Nusselt number ratio of cold to hot flow is also shown as Nu_{r}.

$$Nu_{\mathrm{r}} = \frac{Nu_{\mathrm{c}}}{Nu_{\mathrm{h}}} \tag{13}$$

Dimensionless temperatures for hot and cold flows were obtained according to Eqs. (14) and (15), respectively. In these equations, T_{s} is the temperature obtained from the simulation and T_{∞} is the ambient temperature.

$$\theta_C^* = \frac{T_s - T_{\infty}}{T_{\mathrm{C,i}} - T_{\infty}} \tag{14}$$

$$\theta_H^* = \frac{T_{\mathrm{H,i}} - T_{\infty}}{T_{\mathrm{s}} - T_{\infty}} \tag{15}$$

For numerical solution, the finite volume method based on the SIMPLE algorithm is used. Modeling is done in absolute convergence conditions, and the condition of convergence with residual value is considered for all nonlinear equations as 1×10^{-6}.

Boundary conditions

For the hot flow through the inner tube of the studied geometries, the Reynolds number and the temperature are considered as $\mathrm{Re} = 1800$ and $T_{\mathrm{H,i}} = 353$ K, respectively. The cold flow through the outer tube is investigated for temperature $T_{\mathrm{C,i}} = 298$ K and $200 \leq \mathrm{Re} \leq 1800$. The outer tube is considered as insulation, the inner and outer surfaces of the tube are considered as the contact surface for heat transfer.

Optimization procedure

The Topsis method, as a multi-objective optimization technique, is applied to optimize the performance of the proposed systems from a numerical result viewpoint [53]. In this technique, appropriate solutions are presented based on the behavior of different parameters. Accordingly, in this study, the optimal value of the input parameter (Reynolds number) is achieved based on the desired amount of Nusselt number and Pressure drop as objective functions. The equations for the Topsis optimization method are given in Appendix B.

The Topsis method is used as multi-objective optimization. In multi-objective Topsis optimization, the optimal point has the longest distance from the non-ideal point and the shortest distance from the ideal point. The ideal point is defined as the maximum Nusselt number while the maximum pressure drop is considered as a non-ideal point. Therefore, the objective functions of the multi-objective optimization problem are defined as follows:

$$F_1 = \text{Nusselt number} \tag{16}$$

$$F_2 = \frac{1}{\text{Pressure drop}} \tag{17}$$

Figure 4 shows the flowchart of modeling and optimization procedure in this study. As shown, at first, the modeling parameters including the input Reynolds number and T_{in} are given to the Numerical simulation. Then, validation and mesh independence of the numerical result has been investigated. According to the results, the most effective geometry in improving heat transfer is selected. After it, the Reynolds number of inlet flow is optimized based on Nusselt number and Pressure drop analysis using Topsis-based multi-objective optimization, and finally, the optimal condition is achieved for the best Geometry.

Results

Generally, in the results section, first of all, validation and independence from the numerical simulation grid are discussed. Then, the fluid flow results, including speed distribution and pressure drop, are studied. In the following, the thermal results, including temperature distribution and the variation of the Nusselt number, are performed as the most major heat transfer parameters. Finally, a comparison is made between the three heat exchanger geometries, and the optimization is done to select the optimal possible state for the fluid inlet flow rate with the least amount of pressure drop and the maximum ratio of heat transfer.

Validation and Grid independency

In order to validate the results obtained from numerical simulations. The value of the Nusselt number for the flow inside the inner tube of geometry B with the oil fluid is compared with the numerical results obtained in [30] and the experimental results in [54]. Figure 5 shows the variations of the Nusselt number in different Reynolds numbers to validate the Nusselt number. The absolute average deviation (ADD) was used to calculate the difference between the results of the present work and the reference article. According to Fig. 5, the AAD error is 7.13%, which had an acceptable correlation between the results of the present study and the reference [30] in similar conditions. In addition, Fig. 5 shows that the results of the present study are more consistent with the experimental results than the numerical results [30].

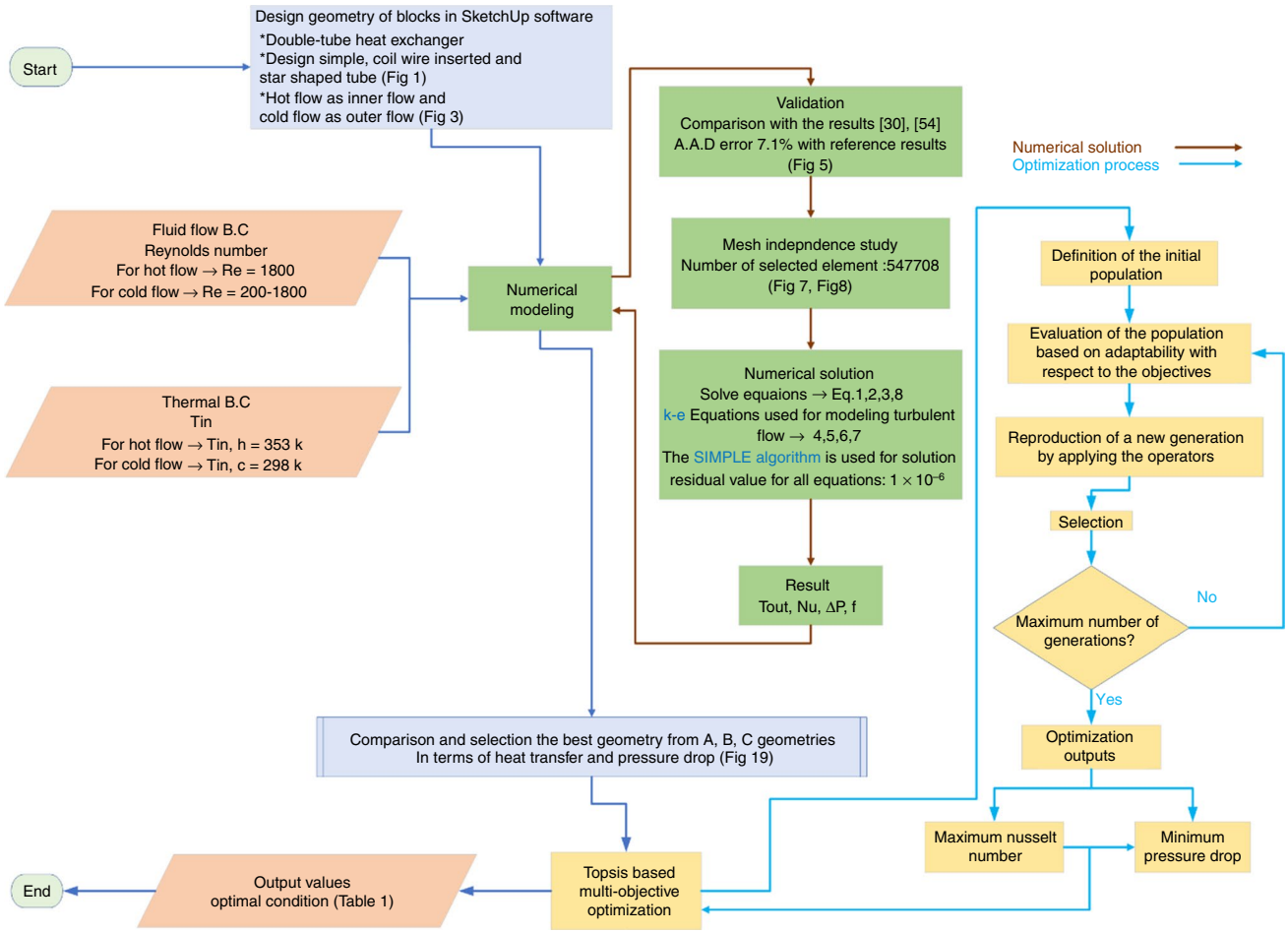

Fig. 4 Flowchart of modeling and optimization procedure

To further validate the present work, the velocity distribution contour according to Fig. 6 is shown in Re = 90 from the numerical work [30] in A and the numerical results from the simulation in the present study in B. According to Part B in Fig. 6, the effect of the turbulator on the velocity contour is visible. Similar to Part A, the tubular causes curvature in the flow lines. A_S can be seen, the trend of the variation of the velocity and flow is like to the reference [30] under the same conditions.

Figure 7 shows the meshes used in the present work for different geometries. The boundary layer mesh in these areas is used due to the drastic changes in flow and heat parameters in the contact area between the two hot and cold fluids and the importance of proper meshing in this area. In geometry B, unstructured meshes are used due to the use of a turbulator in the hot water flow and the complexity of the computational domain geometry.

According to Fig. 8, to investigate the independence of the simulated grid, the effect of variations in the number of elements used in geometry A on the heat transfer coefficient in the cold flow direction of the heat exchanger and logarithmic changes in temperature at the beginning and end of the heat exchanger is studied. Numerical simulations were performed for the number of elements 22,532 to 1,106,011. By increasing the number of elements, both h_c and ΔT_{lm} diagrams show an uptrend, according to Fig. 8. With the number of elements 22,532 to 547,708, the difference between h_c and ΔT_{lm} values is increased at first, but with increasing the number of elements decreases. In the number of elements greater than 547,708, the results are obtained with changes of less than 0.001 and 0.01% for the logarithmic temperature difference and the heat transfer coefficient, respectively; therefore, the computational grid with 547,708 elements is also studied.

Fluid flow results

The variation of the coefficient of friction in terms of the Reynolds number on the cold side of the heat exchanger flow for three different geometries is shown in Fig. 9a. Due to the similarity of the cold flow path geometry for geometries A and B, the friction coefficient diagram for these two

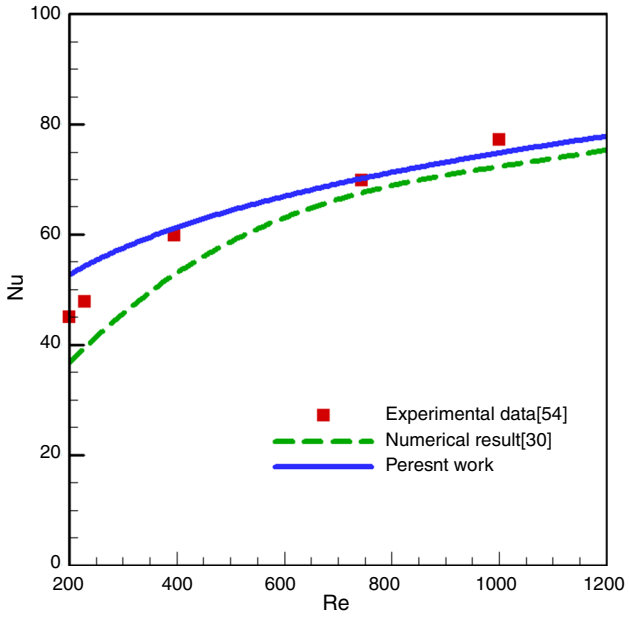

Fig. 5 Validation of the Nusselt number under the same operating conditions with [30] and [54] at different Reynolds numbers for fluid flow from tube with coiled wire turbulator with a pitch of 65 mm and 2 mm diameter

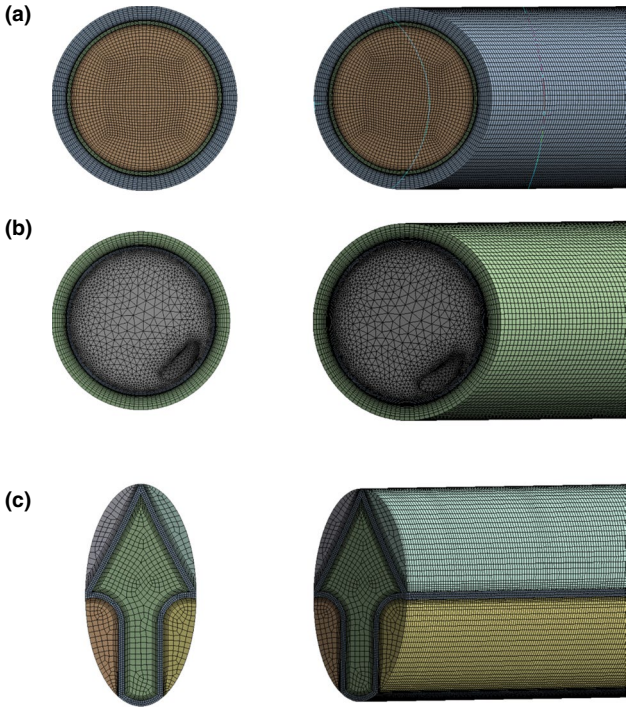

Fig. 7 Created meshes for geometries A, B, C

diagrams is consistent with each other. In geometry C, due to the different cold flow path geometry, the coefficient of friction is shown more diminutive than the other two geometries According to Fig. 9a, by increasing the Reynolds number, the coefficient of friction for all geometries decreases. The maximum value of the coefficient of friction in cold flow was obtained for geometries A and B equal to 0.039, and geometry C equal to 0.013 at Re = 200. The minimum value of F_c for geometries A and B is 0.005 and for geometry C is 0.02 at Re = 1800. The ratio of the variations of the friction coefficient on the cold side of the flow in geometries B and C to the geometry of A is shown in Fig. 9b by increasing the Reynolds number, the diagram is shown slight variations in $f_{r\text{-}c}$. It is considered to be approximately constant for both B and C geometries. According to Fig. 9b, due to the same flow path geometry in geometries A and B, $f_{r\text{-}c}$ for geometry B is shown a fixed-line with a value of 1. According to geometry diagram C, the pressure drop is up to 68% which has decreased Compared to the other two geometries.

The variation of the coefficient of friction in terms of the variation of the Reynolds number in the cold flow for the hot side of the flow in different geometries is shown in Fig. 10a. Because the Reynolds number is constant on the hot side of the heat exchanger, f_h represents constant values for different geometries. The coefficient of friction in geometry A and C are approximately the same value and equal to 0.007, but in geometry B, due to the use of a coiled wire turbulator in the flow path, the coefficient of friction is increased up to 6 times compared to other geometries and is equal to 0.046. The ratio of the coefficient of friction of the hot side of the flow in geometries B and C to the coefficient of the friction in geometry A in different Reynolds numbers of cold flow is

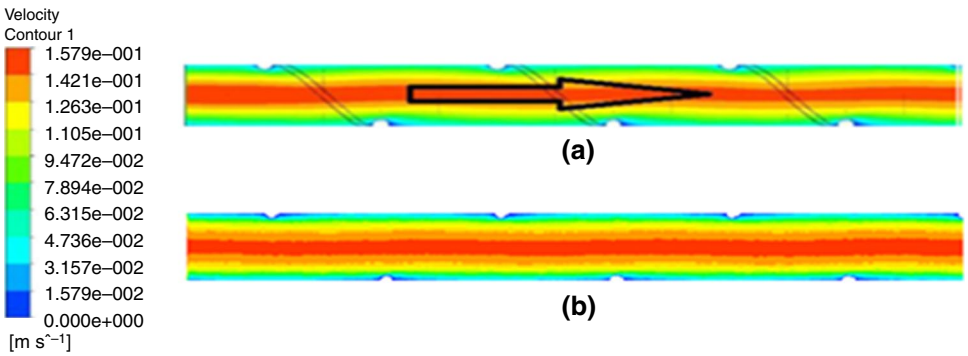

Fig. 6 **a** Comparison of velocity contour in [30]. **b** present work at Re = 90 when using the coiled wire turbulator with a pitch of 65 mm and 2 mm diameter

shown in Fig. 10b. By increasing the Reynolds number, the $f_{r\text{-}h}$ in geometry B increases slightly to 6.7 units at best and Re = 1800. The diagram of C geometry is almost constant and shows that increasing the Reynolds number of the cold flow is almost ineffective at amount $f_{r\text{-}h}$. The coefficient of friction in this geometry, at most, up to 20%, shows a value less than the coefficient of friction in geometry A.

The variation of pressure in the longitudinal direction in the heat exchanger of geometries A, B, and C is shown in Fig. 11, where cold-flow with Re = 200 and hot-flow with Re = 1800 flow inside the tube. The pressure drop for geometry B is greater than other geometries in both cold and hot flow. The higher-pressure drop is obtained in the hot flow path of geometry B compared to the other two geometries. The pressure drop in the cold flow path is the same for geometries A and B but shows more pressure drop than geometry C. The maximum pressure drop is equal to 360 Pa for cold flow in geometry B and the lowest value is equal to 200 Pa for geometry A. In geometry B, the pressure drop changes linearly due to the same pitch of the turbulator and its diameter, and the flow in the turbulent path is developed. Also, at a shorter longitudinal distance than the other two geometries, the pressure drop is seen as linear. At the same time, the values of pressure drop in the inlet area are nonlinear and become linear with the expansion of the flow. It is worth noting, in the hot flow path due to the constant Reynolds number of the hot flow the pressure drop values are equal to the values observed in Fig. 11.

In order to better compare the pressure drop in the cold flow of the heat exchanger, the longitudinal pressure variations in terms of the Reynolds number of the cold flow in geometries B, A, and C are shown in Fig. 12, respectively.

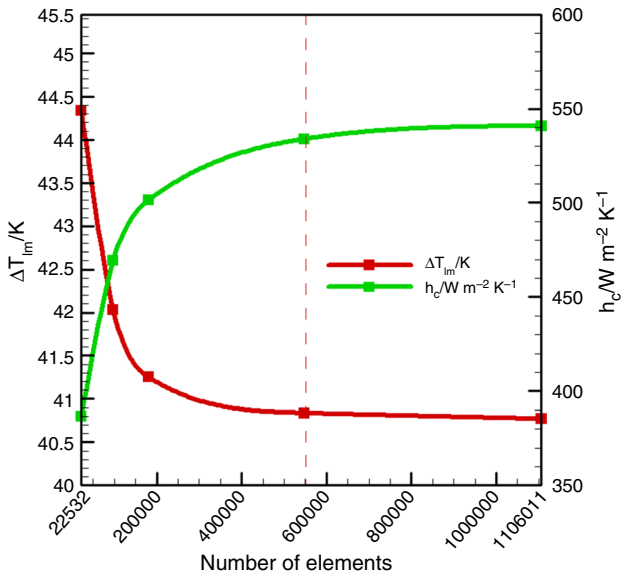

Fig. 8 The independence of the simulation grid for a simple double tube model heat exchanger in hot flow with Re = 1800 and cold flow with Re = 200

By increasing the Reynolds number of the flow in the range of $200 \leq Re \leq 1800$ can be seen an increase in the pressure drop in the path of the tube for all geometries. As the flow moves along the double tube heat exchanger, the flow pressure in geometries A and B decreases as linearly, and because of the same geometry of the flow cross section in these two geometries, Fig. 12a and b is shown the same pressure changes, but Fig. 12-C is shown that it decreases in geometry C as a curve due to the different geometry of

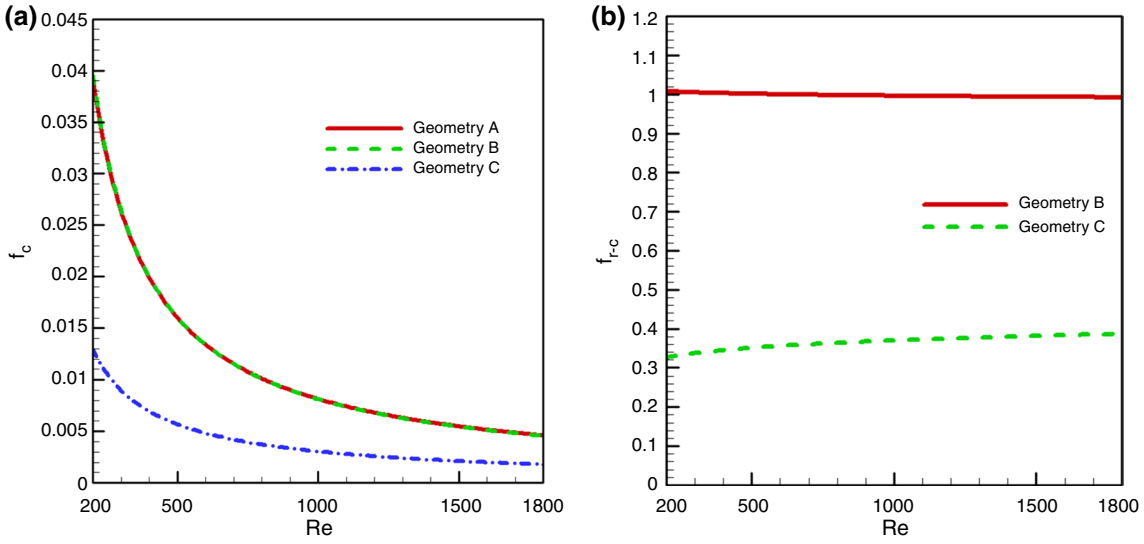

Fig. 9 **a** The Variation of the coefficient of friction in geometries (A, B, C) **b** the ratio of the coefficient of friction in geometries (B and C) to the coefficient of friction of geometry **a** on the cold flow side of the heat exchanger for different Reynolds numbers

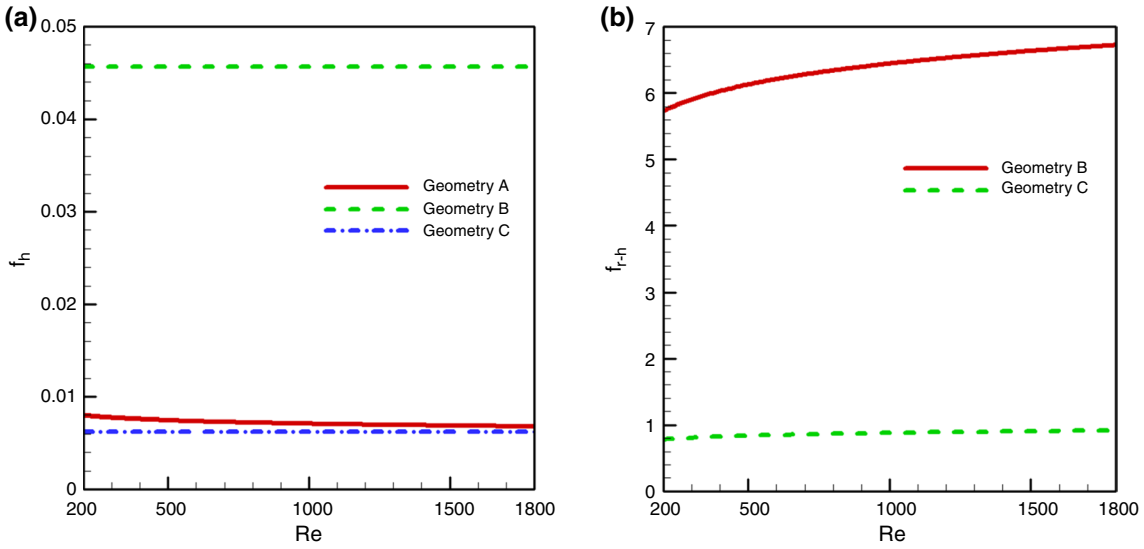

Fig. 10 **a** The variation of the coefficient of friction in geometries A, B, C. **b** The ratio of the coefficient of friction in geometries B and C to the coefficient of friction of geometry A on the hot flow side of the heat exchanger for different Reynolds numbers

the flow cross section. By increasing the Reynolds number, the length of the inlet area increases due to the nonlinearity of the pressure gradient and the cold flow expands at longer distances from the flow inlet it arrives. As shown in Fig. 12, Geometry C causes a lower pressure drop in the fluid flow path than the other two geometries and similar Reynolds number.

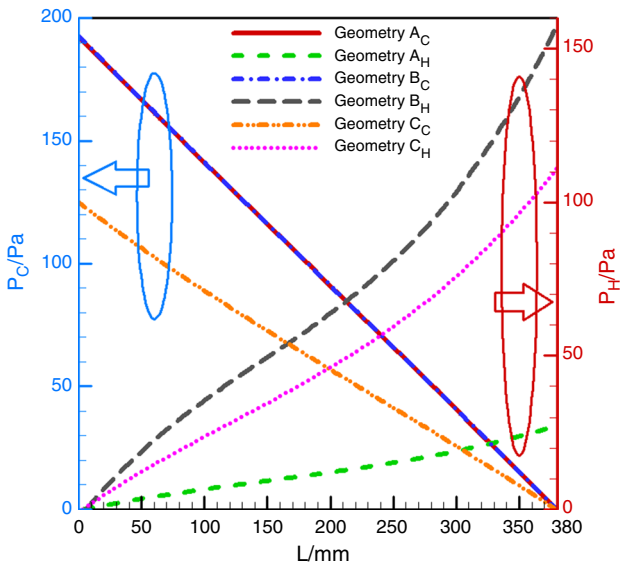

Fig. 11 The variation of pressure in the path of the tube for hot flow with Re = 1800 and Cold flow with Re = 200 in geometries A, B, C

Thermal results

In order to check the thermal parameters in a double tube heat exchanger, the variation of the Nusselt number in terms of Reynolds number in cold flow for different geometries and in conditions where Reynolds number in hot flow is equal to 1800 is shown in Fig. 13a**.** By increasing the Reynolds number, the Nusselt number increases, it is shown an increase in heat transfer in Fig. 13a; in addition, the use of turbulator in hot flow and deformation of the tubes is increased the Nusselt number to 6.1 and 4.2, respectively. Due to the increase in displacement coefficient with increasing Reynolds number, the Nusselt number in these flows is also increased. The ratio of the Nusselt number of cold flows in both geometry B and C to the Nusselt number of the cold flow of simple geometry A is shown in Fig. 13b. The Nusselt number is increased by an average of two times for geometry B and 1.5 times for geometry C compared to simple geometry A, both geometries are performed better with increasing Reynolds number.

The variation of the Nusselt number in terms of the Reynolds number variations in cold flow is shown in Fig. 14a. By increasing the Reynolds number in the cold flow and that the Reynolds number is constant in hot flow, but increases the Nusselt number in geometry A and C and decreases the Nusselt number in geometry B, but these variations are minimal. Another conclusion that can be drawn is that the use of a coil wire increases the Nusselt number for hot flow up to 48, and also the Nusselt number in hot flow in geometry C is reduced by an average of 0.51 times compared to geometry A. Figure 14b shows that the Nusselt number on the hot side of Geometry B is increased by an average of 2 times compared

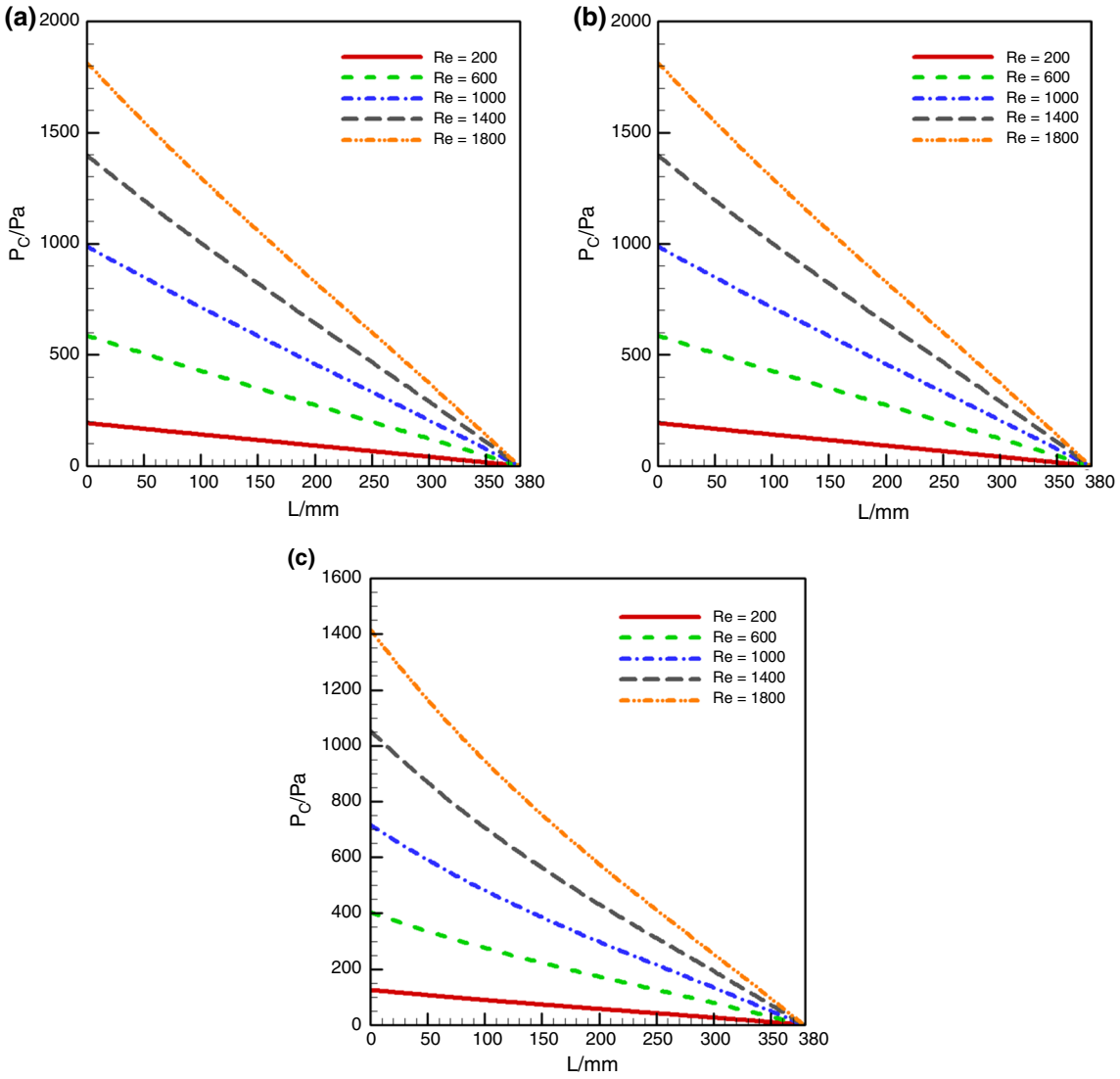

Fig. 12 The variation of the pressure along the length of the tube for cold flow in, **a** geometry A, **b** geometry B, **c** geometry C

to Geometry A, and this value decreased with increasing the Reynolds number. On the other hand, the Nusselt number in geometry B is decreased by an average of 40% compared to geometry A, and by changing the Reynolds number, this ratio remains almost constant.

The ratio of cold flow to hot flow Nusselt numbers in different Reynolds number of the cold flow is shown in Fig. 15. By increasing the Reynolds number, this ratio is almost constant in geometry A and equal to 0.1, but is increased in geometries B and C up to 0.24 and 0.13, respectively. By comparing geometry diagrams B and C, it is clear that geometry C is produced more Nu than geometry B. It is worth that increasing the Nusselt number leads to increasing the heat transfer from hot to cold fluid; according to Fig. 15, this increase in heat transfer at different Reynolds numbers for geometry B and C is approximately constant and equal to 0.12.

The variation of temperature in the path of the tube for hot and cold flows is shown in Fig. 16a. The results of Re = 200 for cold flow and the results of Re = 1800 for hot flow are used in Fig. 14a. According to Fig. 16a, in cold flow, geometry B was able to create up to 80% more temperature difference between the inlet and outlet ports of the tube. For hot flow, regardless of temperature variations in the tube path, geometry B was able to show better performance than geometries C and A again. As it can be concluded that in geometry B, compared to the other two geometries A and C, in addition to lower temperature decrease in hot flow, more temperature increase is created for cold flow. The

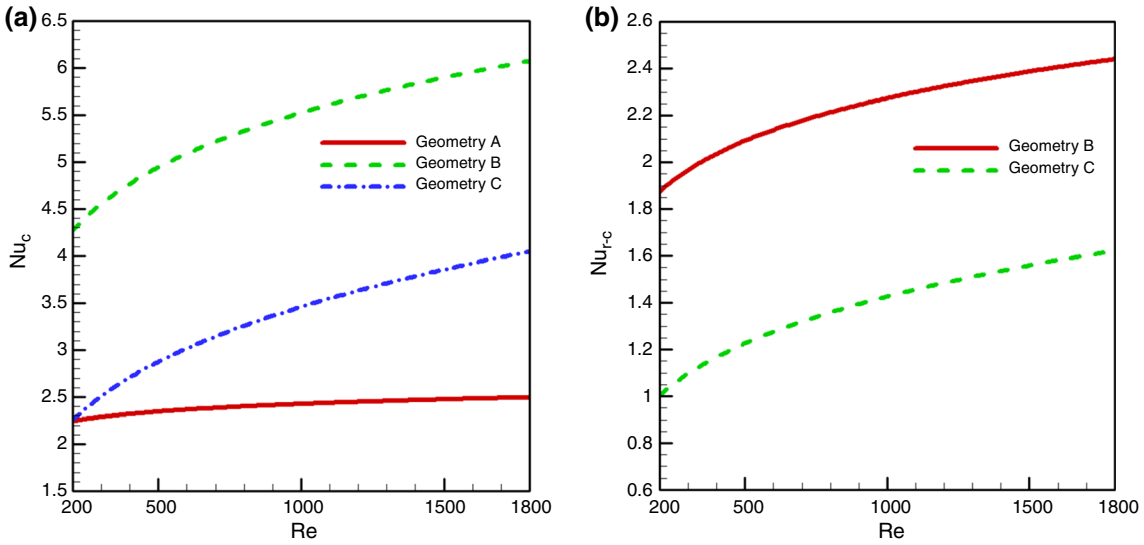

Fig. 13 **a** The variation of the Nusselt number in geometry A, B, and C. **b** The ratio of the Nusselt number in geometry B and C to the Nusselt number in geometry A, on the cold side of the heat exchanger for different Reynolds numbers

variation of temperature in the cold flow side of the flow of geometry B along the length of the tube for $200 \leq Re \leq 1800$ is shown in Fig. 16b. By increasing the Reynolds number, the temperature variations between the inlet and outlet ports of the cold flow are reduced. The results also show that geometry B has better performance for heat transfer and temperature increase than the other two geometries A and C, with increasing the Reynolds number of cold flow in this geometry, the variation of temperature between the input and output ports, dropped to 60% for the Reynolds number 1800. The value of the parameter θ^*_{B-C} in the fluid output section is 10.4 for Re = 200 and 3.6 for Re = 1800.

Comparison and optimization

The temperature contour in different geometries for internal flow (hot) with Reynolds 1800 and external flow (cold) with Reynolds 200 is shown in Fig. 17. The result of using a Turbulator or variation of the shape geometry of the tube in increasing the temperature and heat transfer can be seen

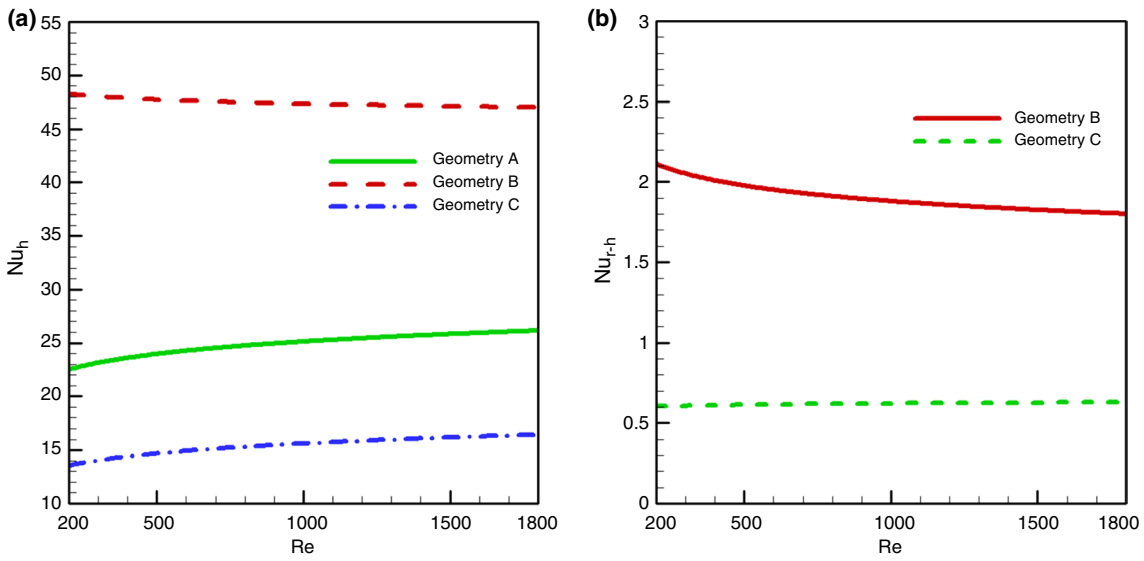

Fig. 14 The variation of the Nusselt number in geometries A, B, and C. **b** The ratio of Nusselt number in geometries B and C to Nusselt number in geometry A, on the hot flow side of the heat exchanger for different Reynolds numbers

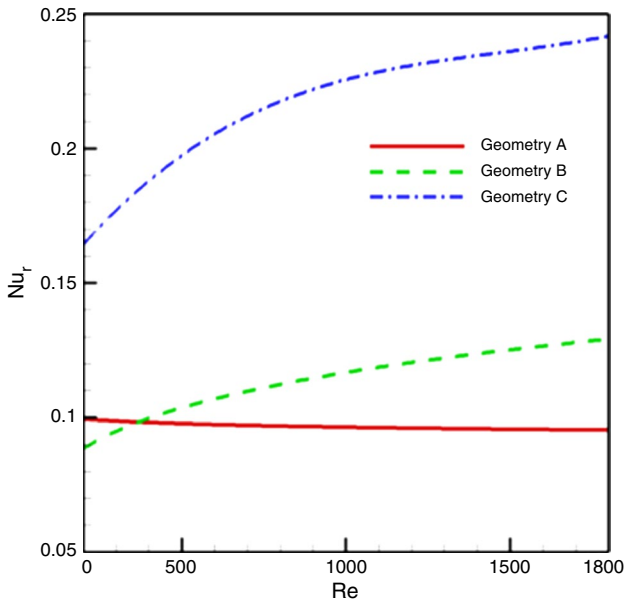

Fig. 15 The ratio of cold flow Nusselt number in $200 \leq Re \leq 1800$ to hot Nusselt number in Reynolds number 1800 for geometries A, B, and C

deformation of the tube geometry can be seen in the turbulence of the thermal boundary layer. According to Fig. 17, the performance of geometry B and the use of Turbulator are better than geometry C, and the deformation of the tube geometry can be concluded. In Fig. 18, the area average temperature of hot flow is shown for geometries A, B, and C. The Reynolds numbers of cold and hot flow are considered 200 and 1800, respectively.

The variation of the Nusselt number in terms of the pressure difference between inlet and outlet of the cold flow for geometries A, B, and C is shown in the diagram of Fig. 19. To investigate diagram, due to the greater importance of increasing the Nusselt number than decreasing the pressure drop, geometry B can be selected as the most suitable geometry. To obtain the optimal Reynolds number in geometry B, the multi-criteria decision-making method (TOPSIS) was used. In this analysis, the two criteria of pressure drop and Nusselt number with different mass percentage effects are investigated in Table (1), and the optimal Reynolds number on the cold flow side was calculated for all three hypotheses proposed, which are in Table (1). The optimal points 1, 2, and 3 for all three assumptions are shown in Fig. 19; the best

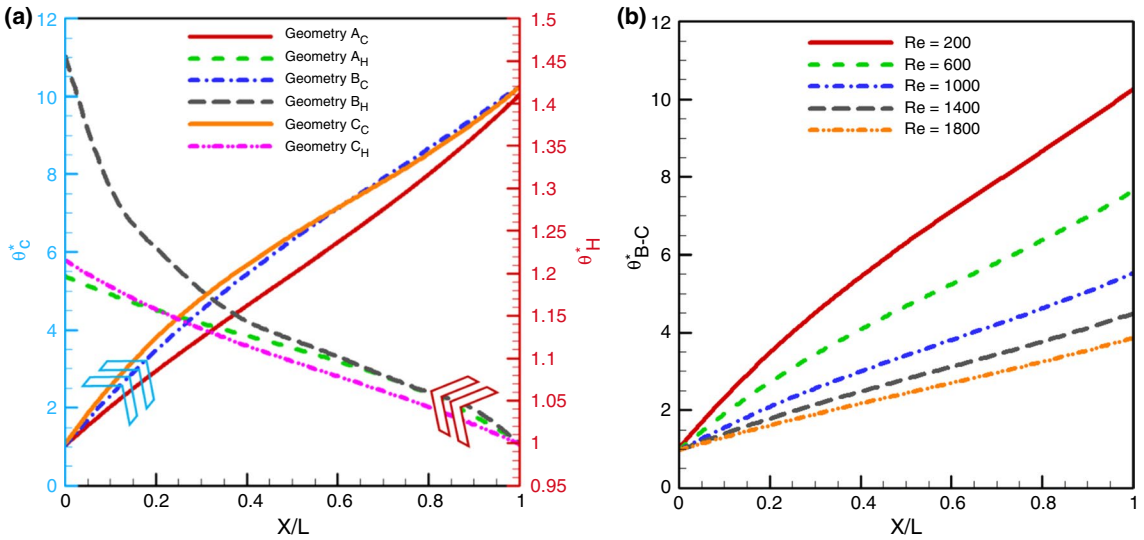

Fig. 16 The variation of dimensionless temperature in the direction of the tube for **a** cold and hot side of the heat exchanger in geometries A, B, and C in Reynolds number 200 and 1800 for cold and hot flow, respectively, **b** geometry B in Reynolds number 1800 for cold flow and hot flow

according to parts A, B, C of Fig. 17. In geometry B, the effect of using a tubular and in geometry C, the effect of

Reynolds values for cold flow are represented in geometry B.

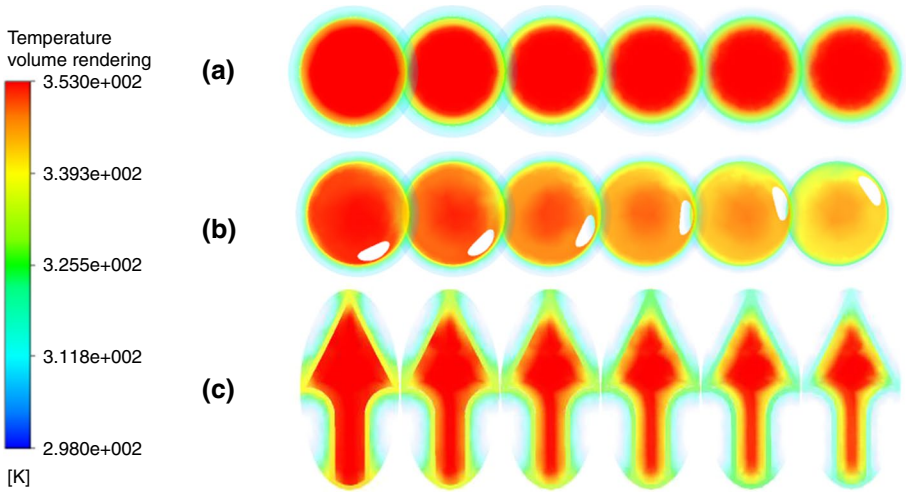

Fig. 17 Temperature contour in geometries A, B, and C for cold flow with Reynolds number 200 and hot flow with Reynolds number 1800

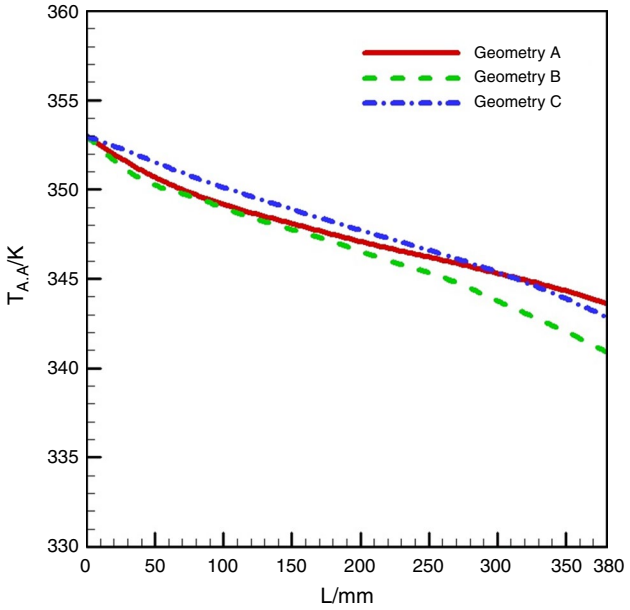

Fig. 18 Area average temperature in hot flows of geometries A, B, and C for cold flow with Reynolds number 200 and hot flow with Reynolds number 1800

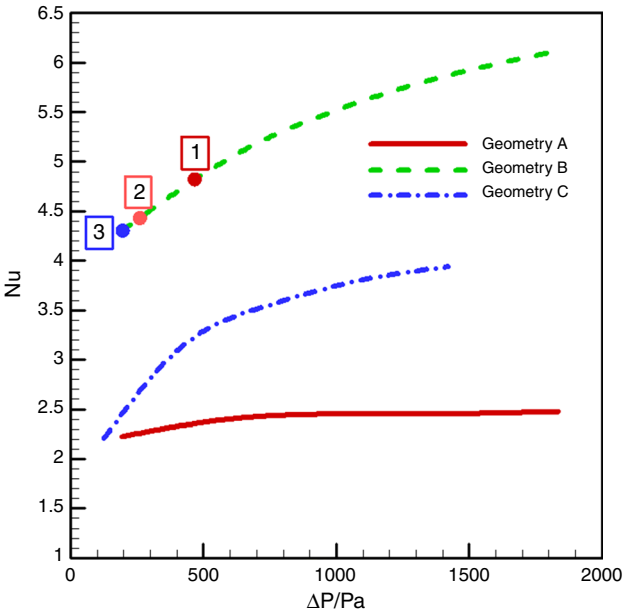

Fig. 19 The variation of the Nusselt number in terms of the pressure difference between the cold inlet and outlet ports for geometries A, B, and C

Table 1 Optimal Reynolds number based on pressure drop and Nusselt number for different mass percentages in geometry B

Assumptions	Hypothesis 1		Hypothesis 2		Hypothesis 3	
Criteria	Nusselt number	Pressure drop	Nusselt number	Pressure drop	Nusselt number	Pressure drop
Type of Criterion	+	−	+	−	+	−
mass percentage of Criterion	70%	30%	50%	50%	30%	70%
The best data	4.8333	468.82	4.4245	258.06	4.3	193.934
Reynolds number obtained	486.09		267.1		200	

Conclusions

In the present study, the effect of different geometries of double tube exchangers, including double tube heat exchanger with circular cross sections in two modes simple and with turbulator and double tube with star-shaped cross section on the variation in forced heat transfer coefficient and the Nusselt number are investigated as parameters of heat transfer and the variation of the pressure drop and friction coefficient are analyzed as parameters of the flow. The Reynolds number is considered for the internal flow of the tube (hot) with an inlet temperature $T_{H,i} = 353$ k constant of $Re = 1800$ and the external flow of the tube (cold) with the inlet temperature $T_{C,i} = 298$ k in the $200 \leq Re \leq 1800$ range. To better model the flow regime and thermal boundary layer in turbulator geometry (Geometry B), standard turbulence equations $k - \varepsilon$ are used to solve Navier–Stokes and energy equations by simple algorithms. To solve the governing equations, the finite volume method based on the SIMPLE algorithm in the fluent solver is used. The average difference of 7.6% between the results of numerical simulation and the results of the reference article has been achieved in the validation section. The length (L) and the thickness of the tube (t) in all geometries are 380 mm and 0.5 mm, respectively. The size of the inlet cross section of the flow inside the tube in the hot and cold sides of the heat exchanger is designed to be the same for all geometries. The main results of this study are summarized as follows.

- Increase in the Nusselt number for all three heat exchanger geometries by increasing Reynolds number and improving the Nusselt number in geometries B and C up to 146% and 50% compared to geometry A, respectively
- Slight effect of increasing the Reynolds number in cold flow on the amount of Nusselt number in hot flow and increasing the Nusselt number of hot flows in Reynolds number 1800 for cold flow up to 8% in geometry A and the best state
- Better thermal performance and more increase in Nusselt number in geometry B than geometry C
- Lower pressure drop also 1.9-folds reduction in coefficient of friction on the cold side of the flow for geometry C compared to geometries A and B with an increase in the Reynolds number of the cold flow
- The coefficient of friction is almost the same for geometries A and C and increases up to 4.8 times in geometry B for internal the tube flow
- Selection of geometry B as the best geometry to increase heat transfer efficiency due to the variation of the pressure drop and Nusselt number and the better effect of using turbulator in increasing Nusselt number by considering pressure drop, compared to tube deformation method and increase the contact surface
- Selection of Reynolds number 486.09 as the optimal working condition for cold flow in geometry B, by using the Topsis method, as a multi-objective optimization technique and according to two criteria of pressure drop with mass percentage -30% and Nusselt number with mass percentage + 70%

Appendix A

Hydraulic diameter (D_H) calculated in Eq. (A-1) which A is the area of the tube surface which the desired flow passes. S is the perimeter of the cross-sectional around which the flow wet it.

$$D_H = \frac{4A}{S} \tag{A.1}$$

The Reynolds number (Re) is also calculated in Eq. (A-2). In this formula, μ is the dynamic viscosity of the fluid flow, which is water.

$$Re = \frac{\rho V D_H}{\mu} \tag{A.2}$$

Appendix B

For the Topsis method, multi-objective optimization can be conducted as follows equations:

$$\text{Max } F_n \quad n = 1, 2, 3, \ldots, N \tag{B.1}$$

$$\text{Subject to } g_j(x) > 0 \quad j = 1, 2, 3, \ldots, j \tag{B.2}$$

$$H_k(x) = 0 \quad k = 1, 2, 3, \ldots, K \tag{B.3}$$

$$x_i^L \leq x_i \leq x_i^U, \quad i = 1, 2, 3, \ldots, n \tag{B.4}$$

where x, n, x_i^L and x_i^U are optimal variables, decision variable vector, lower and upper boundary layer limits, respectively.

References

1. Salimi M, Faramarzi D, Hosseinian SH, Gharehpetian GB. Replacement of natural gas with electricity to improve seismic service resilience: An application to domestic energy utilities in Iran. Energy. 2020. https://doi.org/10.1016/j.energy.2020.117509.

2. Shahzad MW, Burhan M, Li A, Ng KC. Energy-water-environment nexus underpinning future desalination sustainability. Desalination. 2017. https://doi.org/10.1016/j.desal.2017.03.009.
3. Ebrahimi-Moghadam A, Kowsari S, Farhadi F, Deymi-Dashtebayaz M. Thermohydraulic sensitivity analysis and multi-objective optimization of Fe3O4/H2O nanofluid flow inside U-bend heat exchangers with longitudinal strip inserts. Appl Therm Eng. 2020. https://doi.org/10.1016/j.applthermaleng.2019.114518.
4. Azizi Z, Rostampour R, Jafarmadar S, Khorasani S, Abdzadeh B. Performance evaluation of horizontal straight tube equipped with twisted tape turbulator, with air–water two-phase flow as working fluid. J Therm Anal Calorim. 2021. https://doi.org/10.1007/s10973-021-10809-z.
5. Zaboli M, Nourbakhsh M, Ajarostaghi SSM. Numerical evaluation of the heat transfer and fluid flow in a corrugated coil tube with lobe-shaped cross-section and two types of spiral twisted tape as swirl generator. J Therm Anal Calorim. 2020. https://doi.org/10.1007/s10973-020-10219-7.
6. Singh SK, Sarkar J. Improving hydrothermal performance of double-tube heat exchanger with modified twisted tape inserts using hybrid nanofluid. J Therm Anal Calorim. 2020. https://doi.org/10.1007/s10973-020-09380-w.
7. Ebrahimi-Moghadam A, Gohari F, Hoseinzade D, Deymi-Dashtebayaz M. A comprehensive thermo-hydraulic analysis and optimization of turbulent TiO2/W-EG nano-fluid flow inside double-pipe heat exchangers with helical coil inserts. J Braz Soc Mech Sci Eng. 2020. https://doi.org/10.1007/s40430-020-02320-7.
8. Shafee A, Sheikholeslami M, Jafaryar M, Babazadeh H. Hybrid nanoparticle swirl flow due to presence of turbulator within a tube. J Therm Anal Calorim. 2020. https://doi.org/10.1016/10.1007/s10973-020-09570-6.
9. Sheikh R, Gholampour S, Fallahsohi H, Goodarzi M, Taheri MM, Bagheri M. Improving the efficiency of an exhaust thermoelectric generator based on changes in the baffle distribution of the heat exchanger. J Therm Anal Calorim. 2020. https://doi.org/10.1007/s10973-019-09253-x.
10. Zhe T, et al. Turbulent flows in a spiral double-pipe heat exchanger. Int J Numer Meth Heat Fluid Flow. 2019. https://doi.org/10.1016/10.1108/hff-04-2019-0287.
11. Goodarzi M, et al. Investigation of heat transfer and pressure drop of a counter flow corrugated plate heat exchanger using MWCNT based nanofluids. Int Commun Heat Mass Transfer. 2015. https://doi.org/10.1016/j.icheatmasstransfer.2015.05.002.
12. Bahmani MH, Akbari OA, Zarringhalam M, Shabani GAS, Goodarzi M. Forced convection in a double tube heat exchanger using nanofluids with constant and variable thermophysical properties. Int J Numer Meth Heat Fluid Flow. 2019. https://doi.org/10.1108/hff-01-2019-0017.
13. Bahmani MH, et al. Investigation of turbulent heat transfer and nanofluid flow in a double pipe heat exchanger. Adv Powder Technol. 2018. https://doi.org/10.1016/10.1016/j.apt.2017.11.013.
14. Deymi-Dashtebayaz M, Rezapour M. The effect of using nanofluid flow into a porous channel in the CPVT under transient solar heat flux based on energy and exergy analysis. J Therm Anal Calorim. 2020. https://doi.org/10.1007/s10973-020-09796-4.
15. Hosseini SM, Safaei MR, Estellé P, Jafarnia SH. Heat transfer of water-based carbon nanotube nanofluids in the shell and tube cooling heat exchangers of the gasoline product of the residue fluid catalytic cracking unit. J Therm Anal Calorim. 2019. https://doi.org/10.1007/s10973-019-08813-5.
16. Anitha S, Safaei MR, Rajeswari S, Pichumani M. Thermal and energy management prospects of γ-AlOOH hybrid nanofluids for the application of sustainable heat exchanger systems. J Therm Anal Calorim. 2021. https://doi.org/10.1007/s10973-021-10996-9.
17. Bahiraei M, Kiani Salmi H, Safaei MR. Effect of employing a new biological nanofluid containing functionalized graphene nanoplatelets on thermal and hydraulic characteristics of a spiral heat exchanger. Energy Convers Manage. 2019. https://doi.org/10.1016/j.enconman.2018.10.098.
18. Sarafraz M, Safaei M, Tian Z, Goodarzi M, Filho EB, Arjomandi M. Thermal Assessment of Nano-Particulate Graphene-Water/Ethylene Glycol (WEG 60:40) Nano-Suspension in a Compact Heat Exchanger. Energies. 2019. https://doi.org/10.3390/en12101929.
19. Goodarzi M, et al. Investigation of heat transfer performance and friction factor of a counter-flow double-pipe heat exchanger using nitrogen-doped, graphene-based nanofluids. Int Commun Heat Mass Transfer. 2016. https://doi.org/10.1016/j.icheatmasstransfer.2016.05.018.
20. Sarafraz MM, Safaei MR, Goodarzi M, Yang B, Arjomandi M. Heat transfer analysis of Ga-In-Sn in a compact heat exchanger equipped with straight micro-passages. Int J Heat Mass Transf. 2019. https://doi.org/10.1016/j.ijheatmasstransfer.2019.05.057.
21. Li ZX, Khaled U, Al-Rashed A, Goodarzi M, Sarafraz MM, Rashed M. Heat transfer evaluation of a micro heat exchanger cooling with spherical carbon-acetone nanofluid. Int J Heat Mass Transf. 2020. https://doi.org/10.1016/j.ijheatmasstransfer.2019.119124.
22. Alazwari MA, Safaei MR. Combination Effect of Baffle Arrangement and Hybrid Nanofluid on Thermal Performance of a Shell and Tube Heat Exchanger Using 3-D Homogeneous Mixture Model. Mathematics. 2021. https://doi.org/10.3390/math9080881.
23. Giannoni R. Bi- thermal heat exchanger, method and plant for its manufacture. 2010.
24. Abu-Hamdeh NH, et al. A detailed hydrothermal investigation of a helical micro double-tube heat exchanger for a wide range of helix pitch length. Case Stud Therm Eng. 2021. https://doi.org/10.1016/j.csite.2021.101413.
25. Monfared RH, Niknejadi M, Toghraie D, Barnoon P. Numerical investigation of swirling flow and heat transfer of a nanofluid in a tube with helical ribs using a two-phase model. J Therm Anal Calorim. 2021. https://doi.org/10.1007/s10973-021-10661-1.
26. Deymi-Dashtebayaz M, Akhoundi M, Ebrahimi-Moghadam, Arabkoohsar A, Jabari Moghadam AM, Farzaneh-Gord M. Thermo-hydraulic analysis and optimization of CuO/water nanofluid inside helically dimpled heat exchangers. J Therm Anal Calorim. 2020. https://doi.org/10.1007/s10973-020-09398-0.
27. Zekun Y, Yingjie M, Nan Z, Smith R. Design optimization of shell and tube heat exchangers sizing with heat transfer enhancement. Comput Chem Eng. 2020. https://doi.org/10.1016/j.compchemeng.2020.106821.
28. Nakhchi ME, Esfahani JA. Numerical investigation of turbulent CuO–water nanofluid inside heat exchanger enhanced with double V-cut twisted tapes. J Therm Anal Calorim. 2020. https://doi.org/10.1007/s10973-020-09788-4.
29. Shahsavar Goldanlou A, Sepehrirad M, Papi M, Hussein AK, Afrand M, Rostami S. Heat transfer of hybrid nanofluid in a shell and tube heat exchanger equipped with blade-shape turbulators. J Therm Anal Calorim. 2020. https://doi.org/10.1007/s10973-020-09893-4.
30. Khashayar Sharifi KH, Rafiei M, Mohammadi AH, Shirazi L. Computational fluid dynamics (CFD) technique to study the effects of helical wire inserts on heat transfer and pressure drop in a double pipe heat exchanger. Appl Therm Eng. 2018. https://doi.org/10.1016/j.applthermaleng.2017.08.146.
31. Paneliya S, Khanna S, Mankad V, Ray A, Prajapati P, Mukhopadhyay I. Comparative study of heat transfer characteristics of a tube equipped with X-shaped and twisted tape insert. Mater Today Proc. 2020. https://doi.org/10.1016/j.matpr.2020.01.103.

32. Nakhchi ME, Esfahani JA. Cu-water nanofluid flow and heat transfer in a heat exchanger tube equipped with cross-cut twisted tape. Powder Technol. 2018. https://doi.org/10.1016/j.powtec.2018.08.087.
33. Rashidi S, Zade NM, Esfahani JA. Thermo-fluid performance and entropy generation analysis for a new eccentric helical screw tape insert in a 3D tube. Chem Eng Process. 2017. https://doi.org/10.1016/j.cep.2017.03.013.
34. Emani MS, Ranjan H, Bharti AK, Meyer JP, Saha SK. Laminar flow heat transfer enhancement in square and rectangular channels having: (1) A wire-coil, axial and spiral corrugation combined with helical screw-tape with and without oblique teeth and a (2) spiral corrugation combined with twisted tapes with oblique teeth. Int J Heat Mass Transf. 2019. https://doi.org/10.1016/j.ijheatmasstransfer.2019.118707.
35. Yu HZC, Wang Y, Zeng M, Gao B. Numerical study on turbulent heat transfer performance of twisted oval tube with different cross sectioned wire coil. Case Stud Therm Eng. 2020. https://doi.org/10.1016/j.csite.2020.100759.
36. Sinaga N, Khorasani S, Nisar KS, Kaood A. Second law efficiency analysis of air injection into inner tube of double tube heat exchanger. Alexandria Eng J. 2020. https://doi.org/10.1016/j.aej.2020.10.064.
37. Panahi D, Zamzamian K. Heat transfer enhancement of shell-and-coiled tube heat exchanger utilizing helical wire turbulator. Appl Therm Eng. 2017. https://doi.org/10.1016/j.applthermaleng.2016.12.128.
38. Moghaddam HA, Sarmadian A, Shafaee M. An experimental study on condensation heat transfer characteristics of R-600a in tubes with coiled wire inserts. Appl Therm Eng. 2019. https://doi.org/10.1016/j.applthermaleng.2019.113889.
39. Moghaddam HA, Sarmadian A, Shafaee M, Enayatollahi H. Flow pattern maps, pressure drop and performance assessment of horizontal tubes with coiled wire inserts during condensation of R-600a. Int J Heat Mass Transf. 2020. https://doi.org/10.1016/j.ijheatmasstransfer.2019.119062.
40. Raei FSB, Jamialahmadi M, Peyghambarzadeh SM. Different methods to calculate heat transfer coefficient in a double-tube heat exchanger: a comparative study. Exp Heat Transf. 2018. https://doi.org/10.1080/08916152.2017.1341963.
41. Gonzalez JI, Valladares OG, Gordin RG. Experimental study of Heat transfer enhancement for fluid flow inside Annulus with spiral wires. Heat Transfer Eng. 2018. https://doi.org/10.1080/01457632.2017.1280279.
42. He LLY, Li P, Ma L. Experimental study on Heat transfer enhancement characteristics of tube with cross hollow twisted tape inserts. Appl Therm Eng. 2018. https://doi.org/10.1016/j.applthermaleng.2017.12.029.
43. Kumar R, Kumar Pathak A, Kumar M, Kumar Patil A. Experimental study of multi tubular sensible heat storage system fitted with wire coil inserts. Renew Energy. 2020. https://doi.org/10.1016/j.renene.2020.10.058.
44. Sumit SK, Sarkar J. Improving hydrothermal performance of hybrid nanofluid in double tube heat exchanger using tapered wire coil turbulator. Adv Powder Technol. 2020. https://doi.org/10.1016/j.apt.2020.03.002.
45. Keklikcioglu O, Ozceyhan V. Experimental investigation on heat transfer enhancement in a circular tube with equilateral triangle cross sectioned coiled-wire inserts. Appl Therm Eng. 2018. https://doi.org/10.1016/j.applthermaleng.2017.12.051.
46. Moya-Rico JD, Molina AE, Belmonte JF, Córcoles Tendero JI, Almendros-Ibáñez JA. Experimental characterization of a double tube heat exchanger with inserted twisted tape elements. Appl Thermal Eng. 2020. https://doi.org/10.1016/j.applthermaleng.2020.115234.
47. Keklikcioglu O, Ozceyhan V. Entropy generation analysis for a circular tube with equilateral triangle cross sectioned coiled-wire inserts. Energy. 2017. https://doi.org/10.1016/j.energy.2017.07.145.
48. Li F, Zhang X, Wang C, Yang C. Experimental study on gas-liquid flow heat transfer in a horizontal tube with wire-coil inserts. Exp Thermal Fluid Sci. 2017. https://doi.org/10.1016/j.expthermflusci.2017.03.025.
49. Vaisi A, Moosavi R, Lashkari M, Soltani MM. Experimental investigation of perforated twisted tapes turbulator on thermal performance in double pipe heat exchangers. Chem Eng Process. 2020. https://doi.org/10.1016/j.cep.2020.108028.
50. Ribeiro F, de Conde KE, Garcia EC, Nascimento IP. Heat transfer performance enhancement in compact heat exchangers by the use of turbulators in the inner side. Appl Therm Eng. 2020. https://doi.org/10.1016/j.applthermaleng.2020.115188.
51. Goh LHK, Hung YM, Chen GM, Tso CP. Entropy generation analysis of turbulent convection in a heat exchanger with self-rotating turbulator inserts. Int J Therm Sci. 2021. https://doi.org/10.1016/j.ijthermalsci.2020.106652.
52. Shih H. Liou WW. Shabbir TA. Yang Z. Zhu J. A New k-e eddy viscosity model for high reynolds number turbulent flows. Computers Fluid. 1995
53. Nikitin A, Deymi-Dashtebayaz M, Muraveinikov S, Nikitina V, Nazeri R, Farahnak M. Comparative study of air source and ground source heat pumps in 10 coldest Russian cities based on energy-exergy-economic-environmental analysis. J Clean Prod. 2021. https://doi.org/10.1016/j.jclepro.2021.128979.
54. Akhavan-Behabadi MA, Kumar R, Salimpour MR, Azimi R. Pressure drop and heat transfer augmentation due to coiled wire inserts during laminar flow of oil inside a horizontal tube. Int J Therm Sci. 2010. https://doi.org/10.1016/j.ijthermalsci.2009.06.004.